Isı Bilimi ve Tekniği Dergisi, 43, 1, 81-94, 2023
J. of Thermal Science and Technology

ISSN 1300-3615
https://doi.org/10.47480/isibted.1290726

EFFECTS OF ROUGHNESS ELEMENTS ON V-CORRUGATED ABSORBER PLATE SOLAR AIR HEATERS

Hussain SHAWISH[*] and Murat ÖZDENEFE[**]
*Eastern Mediterranean University, Department of Mechanical Engineering
Famagusta, North Cyprus via Mersin 10, Turkey
hussain.shawish@emu.edu.tr, ORCID: 0000-0001-9930-5258
**Eastern Mediterranean University, Energy Research Center
Famagusta, North Cyprus via Mersin 10, Turkey
murat.ozdenefe@emu.edu.tr, ORCID: 0000-0002-8905-0885

(Geliş Tarihi: 20.08.2022, Kabul Tarihi: 31.03.2023)

Abstract: Solar air heaters (SAHs) generally have low thermal efficiency, hence numerous research has been done to enhance their performance and to widen their applications. Although there has been extensive research on them, adding roughness elements on the corrugations of V-corrugated absorber plate SAHs to enhance their performance have not been investigated. Hence this work is an effort to address this gap by performing a numerical study to investigate the thermal performance enhancement caused by attaching transverse and longitudinal fins on 60º V-corrugated absorber plate SAH. It is also aimed to investigate the effect of same roughness elements on simple flat plate SAH. ANSYS Fluent program was utilized to simulate and analyze the three-dimensional airflow through the SAHs. The simulations were performed for three different Reynolds numbers; 4000, 8000 and 12000. The effects of adding fins on the outlet air temperature, Nusselt number and friction factor were analyzed and discussed. The results indicated that addition of roughness in the form of transverse and longitudinal fins offered enhancement in the thermal performance, leading the corrugated plate-longitudinal fins SAH to achieve the maximum outlet air temperature (315.3 K) and the flat plate-transverse fins SAH to attain the highest Nusselt number (58.4). For the V-corrugated SAH, transverse fins enhanced the Nusselt number by 17% compared to the smooth case, while the longitudinal fins offered 4 degrees increase in the outlet temperature. For the flat SAH on the other hand, transverse fins enhanced the Nusselt number by 26% as compared to the smooth case, while the longitudinal fins resulted in 2 degrees increase in the outlet temperature.
Keywords: solar air heater, thermal performance, numerical investigation

PÜRÜZLÜLÜK ELEMANLARININ V-KAT LEVHALI GÜNEŞ HAVA ISITICILARINA ETKİLERİ

Özet: Güneş enerjili hava ısıtıcıları, genellikle düşük ısıl verimliliğe sahiptir. Dolayısıyla bu cihazların performansını artırmak ve uygulamalarını çoğaltmak için birçok araştırma yapılmıştır. Yapılan kapsamlı çalışmalara rağmen, pürüzlülük elemanlarının V-kat levhalı güneş hava ısıtıcılarının soğurucusuna eklenmesinin performans üzerine etkisi incelenmemiştir. Dolayısıyla bu çalışma, 60º V-kat levhalı güneş enerjili hava ısıtıcısının soğurucusuna pürüzlülük elemanlarının (enine ve boyuna uzanan kanatçıklar) eklenmesinin sağlamış olduğu ısıl performans artışını sayısal yaklaşım kullanarak incelemeyi hedeflemektedir. Aynı pürüzlülük elemanlarının düz levhalı güneş hava ısıtıcısına eklenmesi halinde oluşacak etkiyi araştırmak ayrıca amaçlanmıştır. Çalışmada cihazlardan geçen hava akışının üç boyutlu simülasyonunu ve analizini gerçekleştirmek için ANSYS Fluent yazılımı kullanılmıştır. Simülasyonlar üç farklı Reynolds sayısı için yapılmıştır (4000, 8000 ve 12000). Kanatçıkların çıkış hava sıcaklığı, Nusselt sayısı ve sürtünme katsayısı üzerindeki etkileri analiz edilmiş ve tartışılmıştır. Enine ve boyuna kanatçık biçimindeki pürüzlülük elemanlarının eklenmesinin, ısıl performans artışı sağladığı ve V-kat levhalı boyuna kanatçıklı cihazın en yüksek çıkış havası sıcaklığına (315.3 K), bunun yanında düz levhalı enine kanatçıklı cihazın en yüksek Nusselt sayısına (58.4) ulaştığı belirlenmiştir. V-kat levhalı cihaz için, enine kanatçıklar Nusselt sayısını %17 artırırken, boyuna kanatçıklar çıkış sıcaklığında 4 derecelik artış sağlamıştır. Düz levhalı cihaz için ise enine kanatçıklar Nusselt sayısını %26 artırırken, boyuna kanatçıklar çıkış sıcaklığında 2 derecelik artışa neden olmuştur.
Anahtar Kelimeler: güneş enerjili hava ısıtıcıları, ısıl performans, sayısal inceleme

NOMENCLATURE

A_s	Surface Area of the Absorber [m^2]
c_p	Specific Heat [J/kg.K]
D_h	Hydraulic Diameter [m]
e/D	Relative Roughness Height
g_x	Gravitational Acceleration Component in the X Direction [m/s^2]
g_y	Gravitational Acceleration Component in the Y Direction [m/s^2]

g_z	Gravitational Acceleration Component in the Z Direction [m/s^2]
h	Coefficient of Heat Transfer [W/m^2.K]
k	Thermal Conductivity [W/m.K]
L	SAH Length [m]
$\dot{m}$	Air Mass Flow Rate [Kg/s]
Nu	Nusselt Number [=hL/k]
P	Pressure [Pa]
P/e	Relative Roughness Pitch
Pr	Prandtl Number
q	Heat Flux [W/m^2]
Re	Reynolds Number [=vρD/μ]
T_∞	Air Temperature Far From Absorber Plate [K]
T_i	Inlet Air Temperature [K]
T_o	Outlet Air Temperature [K]
T_o^*	Non-dimensional Temperature [K]
T_p	Average Absorber Plate Temperature [K]
T_w	Wall Temperature of the Absorber Plate [K]
u	Velocity in the X Direction [m/s]
v	Velocity in the Y Direction [m/s]
$\bar{v}$	Mean Velocity of Air [m/s]
W	SAH Width [m]
w	Velocity in the Z Direction [m/s]
f	Friction Factor [=$\Delta P D_h/0.5 L \rho v^2$]
μ	Viscosity of Air [N.s/m^2]
ρ	Density [kg/m^3]
RNG	Re-Normalization Group
SAH	Solar Air Heater
SIMPLE	Semi-Implicit Method for Pressure Linked Equations

INTRODUCTION

One of the simplest methods to exploit solar energy is via solar air heaters (SAHs) (Parsa et al., 2021). SAHs are low-cost, eco-friendly solar thermal systems that convert incident solar energy into useful thermal energy (Amit Kumar & Layek, 2021; Parsa et al., 2021). They are predominantly used for space heating and drying applications (Sureandhar et al., 2021). The conventional SAH is composed of an absorbing plate made normally from a metallic material that absorbs the incident radiation, a channel or duct attached to the absorber through which air passes, glazing cover to decrease loss of heat from the absorber while allowing solar radiation to pass, thermal insulation at sides and back of the collector to reduce the thermal losses and a fan to provide means of airflow inside the duct (Saxena et al., 2015). Figure 1 provides an illustrative diagram of a conventional SAH (Tyagi et al., 2012). The incident radiation is absorbed by the absorber and this causes an increase in the absorber's temperature. When air flows over the plate, forced convection is generated and the flowing air starts to absorb heat from the plate which causes its temperature to rise, then this hot air is conveyed by a duct to provide heating for the desired purpose (Singh Bisht et al., 2018).

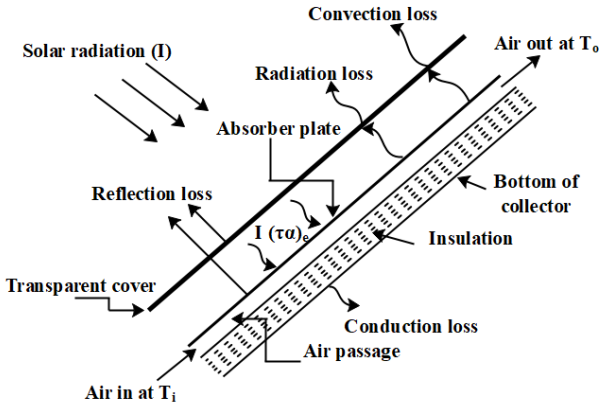

Figure 1. Longitudinal section of a conventional SAH (Tyagi et al., 2012).

Since the working fluid in these systems is air, freezing and boiling does not occur. However, the thermal efficiency of such systems is generally low because of the low heat transfer coefficient values encountered and the poor thermal capacity of air (Ghritlahre et al., 2019). The low heat transfer coefficient is a result of the formation of a laminar viscous layer on the absorber plate causing thermal resistance to heat transfer. Thus the addition of artificial roughness to the absorber plate to break up this layer and generate turbulent flow is a common way to enhance heat transfer coefficient hence the efficiency (Arunkumar et al., 2020). On the other hand, the addition of roughness increases the frictional losses resulting in a higher power requirement for moving the air (Arunkumar et al., 2020).

The thermal and friction characteristics of a shot blasted V-corrugated absorber SAH were studied experimentally by Poongavanam et al. (2018). In their experiments, the authors investigated varying flow rates. The results showed an increase in the mean efficiency as air flow rate increases and the efficiency value in the proposed SAH were higher compared to a smooth flat absorber SAH. In addition, a decrease in friction factor was observed with the increase of mass flow rate. Handoyo et al. (2016) numerically investigated the performance of a V-corrugated absorber SAH with delta-shaped obstacles attached to its backplate. The authors studied the effect of varying obstacles spacing ratio and they achieved optimal Nusselt number and friction factor values at spacing ratio of 1. Analysis on a V-corrugated SAH with twisted tape inserts suspended in the air channel between the absorber and backplate was performed by Farhan et al. (2021). The authors reported a considerable increase in the efficiency as compared to the conventional V-corrugated SAH. Prasad and Saini (1988) studied experimentally the performance in a flat plate SAH with a transverse wire roughness element. The authors investigated the impact of varying relative roughness height on coefficient of heat transfer and friction factor. The results showed that as the relative roughness height increases, the average Nusselt number and friction factor also increase. Performance of a flat plate SAH with transverse wedge-shaped rib roughness geometry was

studied experimentally by Bhagoria et al. (2002). They found an increase in Nusselt number and friction factor with increased relative roughness height. Saini and Saini (1997) tested a flat absorber SAH with expanded metal mesh. They investigated the effect of varying flow rate. The authors found an increase in Nusselt number with rising flow rates, but on the other hand the friction factor decreases. Momin et al. (2002) studied experimentally the performance of a flat absorber SAH with V-shaped roughness geometry. They also found an increase in the performance with increasing relative roughness height for this fin geometry. The effects of different relative roughness height and flow rates on the thermal and friction characteristics of a SAH with dimple-shape roughness were investigated experimentally by Saini and Verma (2008). The results showed good agreement with other studies in the literature. Performance of a SAH with square-sectioned transverse ribs as roughness was studied numerically by Yadav and Bhagoria (2014). They investigated the effects of relative roughness pitch and relative roughness height. A flat plate having discrete multi-V-rib with staggered rib roughness was investigated numerically by Kumar and Kim (2015). The authors studied the effects on performance associated with different relative width ratios for varying Reynolds numbers. The results showed that with an increase in relative width ratios the thermal performance also increased up to an optimum value. Performance of flat plate SAH with inclined circular ribs as the roughness element was studied by Kumar and Varun (2014). The authors investigated the effect of inclination angle and roughness height for different Reynolds numbers. Jin et al (2015) numerically studied a flat absorber SAH with multi V-shaped ribs as roughness. The computations were performed for different roughness parameters to study their effect on Nusselt number and friction factor. Yadav et al. (2014) analyzed numerically the thermal and friction characteristics of a flat absorber SAH with equilateral triangular sectioned rib roughness. The parameters discussed in their study were relative roughness height and relative roughness pitch. A numerical and experimental investigation was performed by Gawanda et al. (2016) to study the performance of a flat absorber SAH having chamfered square ribs attached to the absorber. The authors found an increase in Nusselt number and friction factor with increasing chamfer angle.

Ample of studies have been reported in the literature on the effect of adding different types of fins and roughness geometries to flat absorber plates, however studies investigating the effect of combining artificial roughness elements with the corrugated absorber plates are very few. Handoyo et al. (2016) and Farhan et al. (2021) studied the effects of adding obstacles to the V-corrugated SAHs, however in their studies the obstacles were not attached to the corrugations, rather they were either inserted in the channel between the corrugations and back plate or attached to the back plate. Poongavanam et al. (2018) on the other hand used shot-blasting to create roughness on the corrugations of the V-corrugated SAH. However, the roughness they created are at micron scale. To the best knowledge of the authors, studies investigating thermal and friction characteristics of V-corrugated absorber plate SAH with fins attached directly to the absorber plate do not exist. Therefore, this work strives to numerically investigate and compare the effect of different roughness geometries and airflow rates on the thermal performance of V-corrugated absorber plate SAH with groove angle of 60^o. A further purpose of this work is to employ the same roughness geometries and airflow rates in ordinary flat absorber plate SAH and compare the results.

METHODOLOGY

In the current study a numerical analysis is conducted to investigate the thermohydraulic performance of different types of solar air heaters. ANSYS Fluent CFD code is used to simulate the three-dimensional fluid flow and heat transfer characteristics of the SAHs. This section describes the particulars of the computational domain, grid generation, governing equations, boundary conditions and turbulence model selection.

Computational Domain

In the present study, 6 different SAHs were modeled and simulated. The six SAHs considered in the simulations were for two different types of SAHs; 60^o V-corrugated absorber and flat absorber SAHs. For each type, 3 different designs; smooth plate, plate with transverse fins and plate with longitudinal fins were considered. For each SAH, the computational domain corresponds to the 3D geometry generated by SolidWorks software which is then exported to ANSYS. The length of the considered SAHs is divided into entrance, test and exit sections as proposed in ASHRAE standard 93-2003 (ASHRAE Standard, 2003). A summary of the general geometrical parameters used in the construction of the SAHs is presented in Table 1.

Table 1. General geometric parameters considered for the SAHs.

Entrance section	250 mm
Test Section	300 mm
Exit Section	150 mm
Width (W)	100 mm
Hydraulic Diameter (D_h)	33.33 mm

Two roughness elements i.e. transverse and longitudinal fins were selected since they correspond to different heat transfer enhancement aspects. The transverse fins generate more turbulence in the flow and eliminate the viscous sub-layer, which results in higher heat transfer coefficients. On the other hand, the longitudinal fins mainly offer more surface area, so more air is in contact with the heated surface. The cross-section of both fins is a rectangle having 1mm thickness and 2mm height. Furthermore, all the SAHs are modeled as a single flow duct with its top wall representing the absorber plate of the SAH and the roughness is attached to the bottom side of this absorber plate in the case of roughened SAHs.

The generated 3D models are illustrated in Figures 2A-F. To reduce the computational time, only half of each SAH was considered in the simulations since all SAHs have a symmetry plan at x=W/2. This significantly reduces the number of elements in the mesh and the time required of each simulation while getting the same result as the full SAH case. The working fluid through the whole analysis is air, and the flow is assumed to be 3 dimensional, steady and incompressible. The walls of the SAHs' duct and the absorber plate are assumed to be made of aluminum. Table 2 lists the properties of the materials used in the simulations.

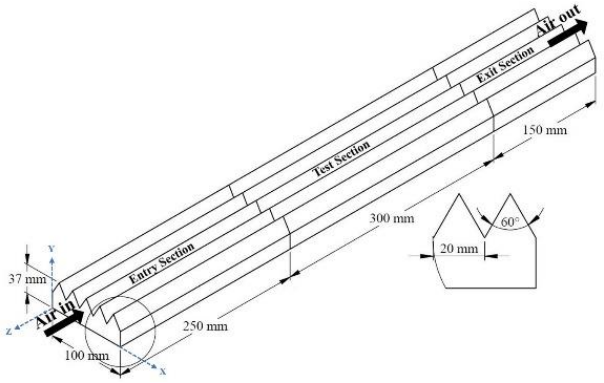

a. Corrugated plate-smooth SAH

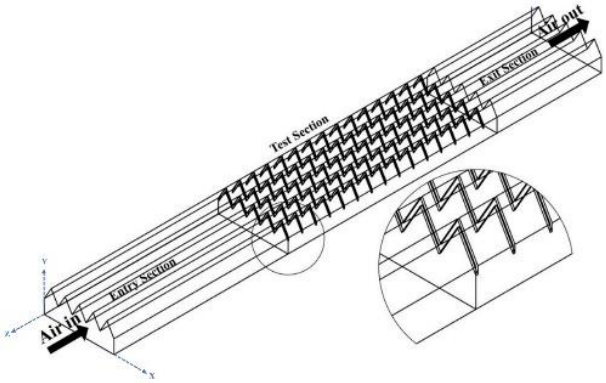

b. Corrugated plate-transverse fins SAH

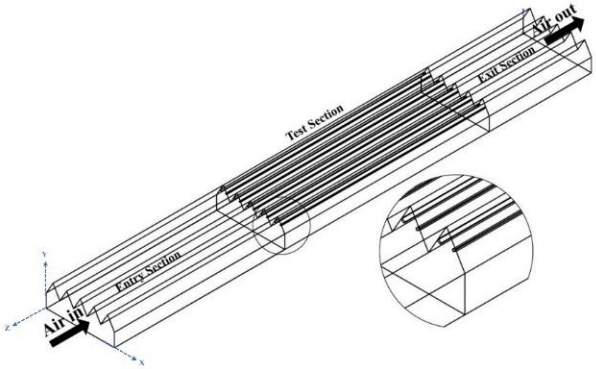

c. Corrugated plate-longitudinal fins SAH

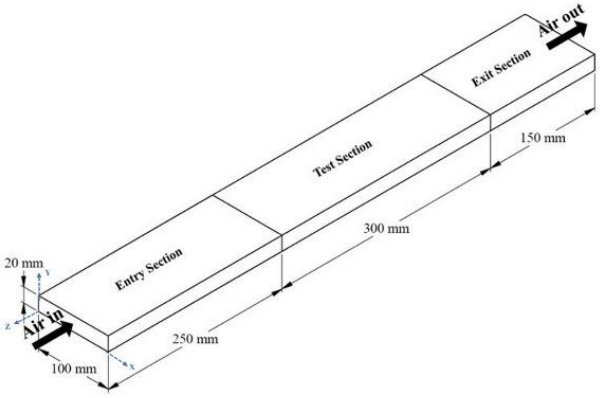

d. Flat plate-smooth SAH

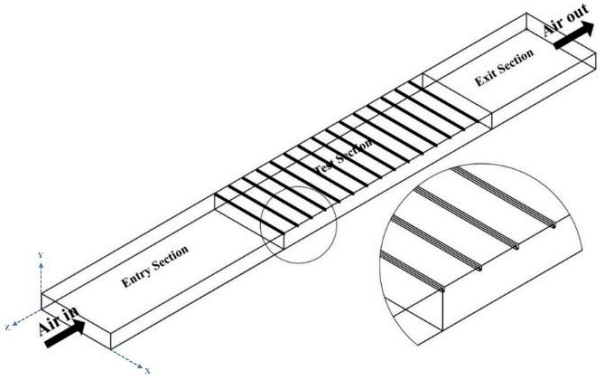

e. Flat plate-transverse fins SAH

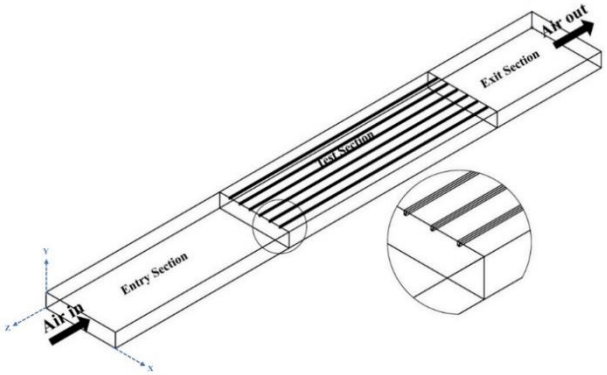

f. Flat plate-longitudinal fins SAH

Figure 2. Generated three-dimensional models

Table 2. Properties of materials used in the simulations

Material	Density ρ (kg/m^3)	Thermal Conductivity k (W/m.K)	Specific Heat c_p (J/kg.K)	Viscosity μ ($N.s/m^2$)	Prandtl Number Pr
Air	1.117	0.0262	1007	1.857e-5	0.71
Aluminum	2719	202.4	871	-	-

Grid Generation

In this study, a non-uniform mesh with prism layers was created for the flow domain of all SAHs using ANSYS meshing. A Mesh independence check was conducted to examine the independency of the generated results from the mesh. Taking the corrugated plate-transverse fins SAH as an example, four meshes with an increasing number of elements from 1457397 to 2503811 corresponding to a decrease in the element size were tested. It was found that a mesh with 1863402 number of elements offered the optimum computational time with less than 1% variation in the results from the mesh with 2503811 elements. Figure 3 shows the generated mesh for the corrugated plat-transverse fins SAH.

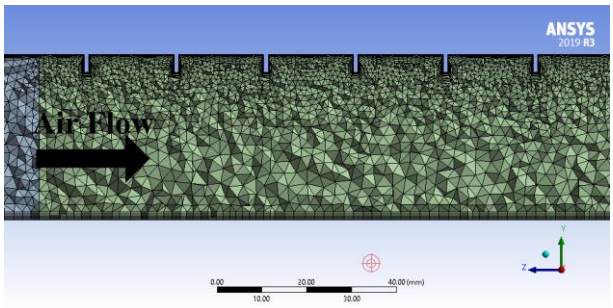

Figure 3. Non-uniform mesh generated for corrugated plate-transverse fins SAH.

Governing Equations

In this work, the aim is to investigate the effect of adding roughness on various parameters such as outlet air temperature, Nusselt number and friction factor that represent the performance of the SAHs. The governing equations of fluid flow are continuity, momentum and energy equations, which can be written as follows (Jiji, 2009):

Continuity equation:

$$\frac{\partial \rho}{\partial t} + u\frac{\partial \rho}{\partial x} + v\frac{\partial \rho}{\partial y} + w\frac{\partial \rho}{\partial z} + \rho\left[\frac{\partial u}{\partial x} + \frac{\partial v}{\partial y} + \frac{\partial w}{\partial z}\right] = 0 \quad (1)$$

Momentum equations:

$$\rho\frac{Du}{Dt} = \rho g_x - \frac{\partial p}{\partial x} + \frac{\partial}{\partial x}\left[\mu\left(2\frac{\partial u}{\partial x} - \frac{2}{3}\nabla\cdot\vec{V}\right)\right] + \frac{\partial}{\partial y}\left[\mu\left(\frac{\partial u}{\partial y} + \frac{\partial v}{\partial x}\right)\right] + \frac{\partial}{\partial z}\left[\mu\left(\frac{\partial w}{\partial x} + \frac{\partial u}{\partial z}\right)\right] \quad (2)$$

$$\rho\frac{Dv}{Dt} = \rho g_y - \frac{\partial p}{\partial y} + \frac{\partial}{\partial y}\left[\mu\left(2\frac{\partial v}{\partial y} - \frac{2}{3}\nabla\cdot\vec{V}\right)\right] + \frac{\partial}{\partial z}\left[\mu\left(\frac{\partial v}{\partial z} + \frac{\partial w}{\partial y}\right)\right] + \frac{\partial}{\partial x}\left[\mu\left(\frac{\partial u}{\partial y} + \frac{\partial v}{\partial x}\right)\right] \quad (3)$$

$$\rho\frac{Dw}{Dt} = \rho g_z - \frac{\partial p}{\partial z} + \frac{\partial}{\partial z}\left[\mu\left(2\frac{\partial w}{\partial z} - \frac{2}{3}\nabla\cdot\vec{V}\right)\right] + \frac{\partial}{\partial x}\left[\mu\left(\frac{\partial w}{\partial x} + \frac{\partial u}{\partial z}\right)\right] + \frac{\partial}{\partial y}\left[\mu\left(\frac{\partial v}{\partial z} + \frac{\partial w}{\partial y}\right)\right] \quad (4)$$

Energy equation:

$$\rho c_p\left(\frac{\partial T}{\partial t} + u\frac{\partial T}{\partial x} + v\frac{\partial T}{\partial y} + w\frac{\partial T}{\partial z}\right) = k\left(\frac{\partial^2 T}{\partial x^2} + \frac{\partial^2 T}{\partial y^2} + \frac{\partial^2 T}{\partial z^2}\right) + \mu\Phi$$

Where

$$\Phi = 2\left[\left(\frac{\partial u}{\partial x}\right)^2 + \left(\frac{\partial v}{\partial y}\right)^2 + \left(\frac{\partial w}{\partial z}\right)^2\right] + \left[\left(\frac{\partial u}{\partial y} + \frac{\partial v}{\partial x}\right)^2 + \left(\frac{\partial v}{\partial z} + \frac{\partial w}{\partial y}\right)^2 + \left(\frac{\partial w}{\partial x} + \frac{\partial u}{\partial z}\right)^2\right] - \frac{2}{3}\left(\frac{\partial u}{\partial x} + \frac{\partial v}{\partial y} + \frac{\partial w}{\partial z}\right)^2 \quad (5)$$

These equations are solved numerically using ANSYS Fluent software. The SIMPLE algorithm was used to handle the coupling in the pressure and velocity fields and the RNG k-ε model was selected as the turbulence model for the simulations. The residuals in the solution of 10^{-3} in momentum and continuity equation and 10^{-6} for energy equation were selected as the convergence criterion. These models were selected based on the validation and application done in previous studies (Gawande et al., 2016; Jin et al., 2015; Anil Kumar & Kim, 2015; Yadav & Bhagoria, 2014). The obtained results from the simulations for the heat transfer coefficient, temperature distribution and pressure are employed to find the aforementioned performance parameters using the following expressions:
The average Nusselt number is defined as

$$Nu = \frac{h\,D_h}{k} \quad (6)$$

Where h is the average coefficient of heat transfer between the absorber plate and air, D_h is the hydraulic

diameter of the SAH and k is the thermal conductivity of air.

The average coefficient of heat transfer h is obtained by surface integrals at the absorber plate and it is defined as

$$h = \frac{q}{T_w - T_\infty} \quad (7)$$

Where q is the wall heat flux, T_w is the wall temperature and T_∞ is the air temperature far away from the wall.

The average friction factor is defined as

$$f = \frac{(\Delta p/L)D_h}{\frac{1}{2}\rho\bar{v}^2} \quad (8)$$

Where Δp is the pressure difference between the inlet and outlet of the SAH, L is the length of the SAH, ρ is the density of air and $\bar{v}$ is the mean air velocity.

Figure 4 presents a flow chart of the methodology that has been followed to generate the results using ANSYS Fluent software.

Boundary Conditions

In the present simulations, the walls in the computational domain were assigned to no-slip condition. At the inlet, a uniform velocity corresponding different Reynolds numbers was applied normal to the boundary with 300 K as the inlet temperature of the air. Three different Reynolds numbers; 4000, 8000 and 12000 were considered. For the outlet, a pressure-outlet condition was assigned where the pressure is equal to the atmospheric pressure. The surface of the absorber plate was assigned with constant heat flux while all other surfaces are assumed to be adiabatic. Moreover, a symmetry boundary condition was applied to the symmetry plane at x=W/2. Table 3 presents a summary of the boundary conditions used.

Table 3. Boundary conditions used in the computational domain.

Surface	**Assigned boundary condition**
inlet	Velocity-inlet
outlet	Pressure-outlet
Absorber Plate	Heat flux
Side and bottom walls of the test section	Adiabatic
Walls of entry and exit sections	Adiabatic
Symmetry plane at x=W/2	Symmetry

Transport Equations for Renormalization-Group (RNG) k-ε Turbulence Model

The RNG k-ε model was derived using a statistical technique called renormalization group theory. It is similar in form to the standard k-ε model but includes some refinements. The RNG model has an additional term in its ε equation that improves the accuracy for rapidly strained flows. Also, the RNG model includes the

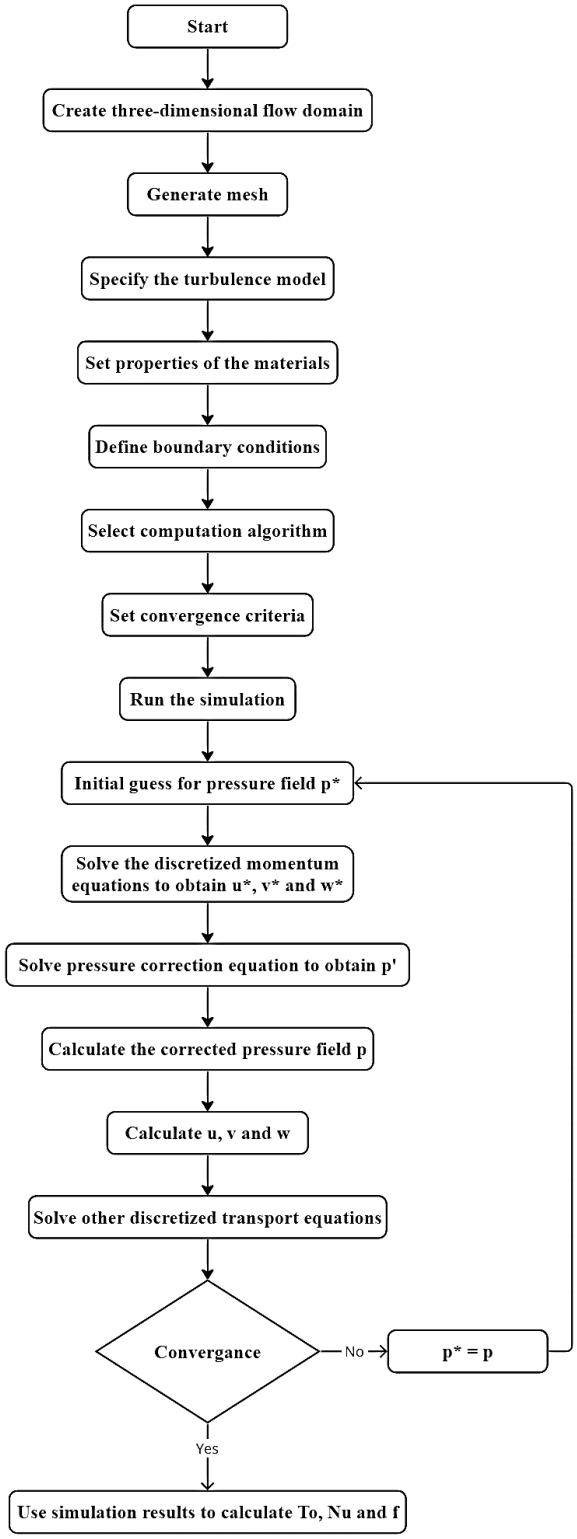

Figure 4. Flow chart of the followed methodology

effect of swirl on turbulence, thus improving the accuracy for swirling flows (ANSYS FLUENT 15, 2013; Yakhot & Smith, 1992). The modeled turbulent kinetic energy, k, and its rate of dissipation ε, are obtained from the following transport equations for the RNG k-ε turbulence model (ANSYS FLUENT 15, 2013; Yadav & Bhagoria, 2014)

$$\frac{\partial}{\partial t}(\rho k) + \frac{\partial}{\partial x_i}(\rho k u_i) = \frac{\partial}{\partial x_j}\left(\alpha_k \mu_{eff} \frac{\partial k}{\partial x_j}\right) + G_k + G_b - \rho\varepsilon - Y_M + S_k \quad (9)$$

$$\frac{\partial}{\partial t}(\rho \varepsilon) + \frac{\partial}{\partial x_i}(\rho \varepsilon u_i) = \frac{\partial}{\partial x_j}\left(\alpha_\varepsilon \mu_{eff} \frac{\partial \varepsilon}{\partial x_j}\right) + C_{1\varepsilon}\frac{\varepsilon}{k}(G_k + C_{3\varepsilon}G_b) - C_{2\varepsilon}\rho\frac{\varepsilon^2}{k} - R_\varepsilon + S_\varepsilon \quad (10)$$

In these equations, G_k represents the generation of turbulence kinetic energy due to the mean velocity gradients and is evaluated by

$$G_k = -\overline{\rho u_i' u_j'}\frac{\partial u_j}{\partial x_i} \quad (11)$$

G_b is the generation of turbulence kinetic energy due to buoyancy and is expressed as

$$G_b = \beta g_i \frac{\mu_t}{Pr_t}\frac{\partial T}{\partial x_i} \quad (12)$$

Y_M represents the contribution of the fluctuating dilatation in compressible turbulence to the overall dissipation rate and is defined as

$$Y_M = 2\rho\varepsilon M_t^2 \quad (13)$$

The quantities α_k and α_ε are the inverse effective Prandtl numbers for k and ε respectively. S_k and S_ε are user-defined source terms.

μ_{eff} represents the effective turbulent viscosity and is given by

$$\mu_{\text{eff}} = \mu + \mu_{\text{t}}$$

where

$$\mu_t = \rho C_\mu \frac{k^2}{\varepsilon} \quad (14)$$

The default values of the model constants $C_{1\varepsilon}, C_{2\varepsilon}, \alpha_k, \alpha_\varepsilon$ and C_μ are equal to 1.42, 1.68, 1.39, 1.39 and 0.0845 respectively.

Validation of the CFD Model

The selected turbulence model is validated by comparing the average Nusselt number values predicted by the CFD model to the values obtained using Dittus-Boelter equation (see Eq. 15) (Incropera & DeWitt, 2007) for smooth SAHs as presented in Figure 5. This is analogous to the validation method used in literature (Yadav & Bhagoria, 2014; Anil Kumar & Kim, 2015). It is clear in the figure that predicted results for corrugated plate are closely agreeing with the results of Dittus-Boelter equation, while the results for the flat plate are overpredicted to a certain extend. The average error in Nusselt number values for corrugated plate smooth and flat plate smooth SAHs from the Dittus-Boelter equation was 9.52% and 32.7% respectively while the average absolute difference was +2.38 and +8.45 respectively.

$$Nu_s = 0.0243 Re_D^{0.8} Pr^{0.4} \quad (15)$$

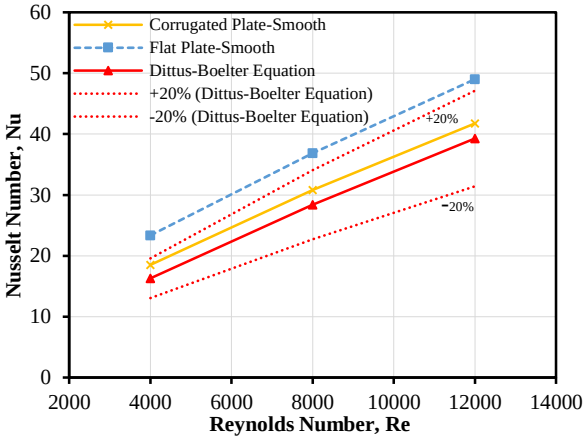

Figure 5. Comparison between the predicted Nusselt number with Dittus-Boelter Equation at different Reynolds numbers

RESULTS AND DISCUSSIONS

Thermohydraulic performance of considered SAH designs i.e., 60° V-corrugated and flat absorber plate with different roughness elements are investigated numerically to reveal the effect of roughness elements on the performance. Outlet air temperature, Nusselt number and friction factor are three principal parameters that are examined and discussed. The results are presented for varying Reynolds numbers. In addition to the results obtained in this study, the available experimental results for Nusselt number and friction factor existing in the literature are also presented as an attempt to further validate the current study. Due to the difficulty of finding studies employing the identical geometric and operating conditions as used in this study, the authors considered available data from research works on flat plate SAHs employing same general aim and range of Reynolds number for the comparisons. Bhagoria et al.(Bhagoria et al., 2002) and Momin et al.(Momin et al., 2002) used the concept of adding roughness to enhance the performance of SAHs which is analogous to the aim of the current study. Bhagoria et al. used wedge shaped, whereas Momin et al. employed V-shaped roughness elements

that are transversely attached to the absorber plate. The range of the Reynolds number considered in their work (2500 to 18000) is similar to the range employed in the present study (4000 to 12000).

Outlet air Temperature

The average outlet air temperature at different Reynolds numbers is presented in Figure 6 for different SAHs considered in this study. For all SAHs, the graph shows a decrease in the outlet temperature of air with increasing Reynolds numbers.

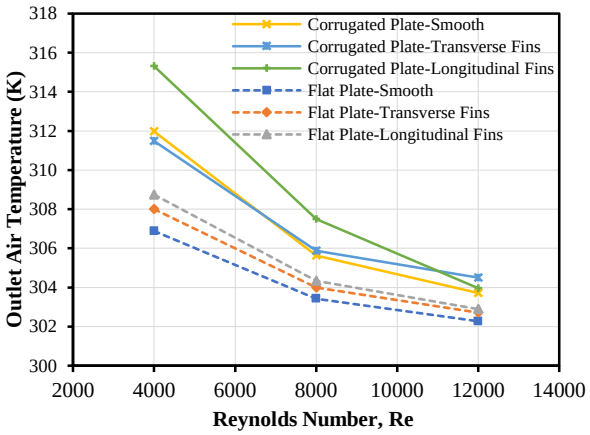

Figure 6. Outlet air temperature against Reynolds number for different SAHs

For V-corrugated SAHs, a maximum outlet temperature of 315.32 K was obtained in longitudinal fins case at Re=4000, while the minimum was 303.7 K in the smooth case corresponding to Re=12000. In addition, it can be seen from the graph that corrugated plate SAHs achieved higher outlet temperatures than flat plate SAHs for the considered Reynolds numbers. This is mainly because the corrugated absorber plate offers considerably more heat transfer surface area than the flat absorber plate, leading more air to be in direct contact with the absorber which results in higher outlet temperatures. Further investigation of the plot shows that at Re=12000, the corrugated plate-transverse fins SAH achieved higher outlet temperature than the corrugated plate-longitudinal fins. This observation raises the idea that at higher Reynolds numbers the effect of increasing the coefficient of heat transfer by transverse fins to achieve higher outlet temperatures surpasses the effect of higher surface area offered by the longitudinal fins.

For flat absorber plate SAHs, the maximum outlet temperature was obtained in the longitudinal fins case which corresponds to 308.7 K at Re=4000, while the minimum value of outlet temperature was 302.3 K in the smooth case for Re=12000. This result is akin to the case of V-corrugated plate. Moreover, it is noted that for all Reynolds numbers considered the SAH with longitudinal fins maintained the highest outlet temperatures among other flat plate SAHs.

To be able to draw general conclusions regarding considered SAHs' effect on the outlet air temperature it is useful to nondimensionalize the air temperature. In this study non-dimensional temperature is defined as the ratio of the actual temperature rise from inlet to outlet to the maximum possible temperature rise (which is the plate temperature minus inlet temperature) as given in equation 16. Hence greater non-dimensional temperature indicates that the outlet air temperature is closer to its maximum possible value which is the plate temperature. Figure 7 displays the relation between the non-dimensional temperature (T_o^*) and Reynolds number for various SAH configurations. SAHs with transverse fins achieved better non-dimensional temperature compared to other configurations. For the first data point (Re=4000), flat plate-transverse fins achieved higher value of non-dimensional temperature compared to corrugated plate-transverse fins case. The non-dimensional temperature can be thought as a performance metrics indicating how effective a certain SAH is achieving the potential maximum temperature increase across the SAH. Hence, higher value of non-dimensional temperature for flat plate-transverse fins compared to corrugated plate-transverse fins for the first data point (Re=4000) means that at this Reynolds number flat plate-transverse fins better utilized the available potential. However, it must be said that the difference is 0.009 which is inconsequential. Since the corrugated plate-transverse fins SAH results in higher outlet temperature, the only reason for having higher dimensionless temperature at Re= 4000 in flat plate-transverse fins case is due to its much lower plate temperature (meaning its potential maximum temperature rise is low) than its counterpart, i.e. corrugated plate-transverse fins case. The variations in T_o^* values among the other SAHs (corrugated plate smooth, corrugated longitudinal fins, flat plate smooth and flat plate longitudinal fins) are minimal, making it difficult to draw a conclusive remarks regarding which is better. However, it can be said that corrugated plate smooth and corrugated longitudinal fins performed slightly better than their flat plate counterparts.

$$T_o^* = \frac{T_o - T_i}{T_p - T_i} \tag{16}$$

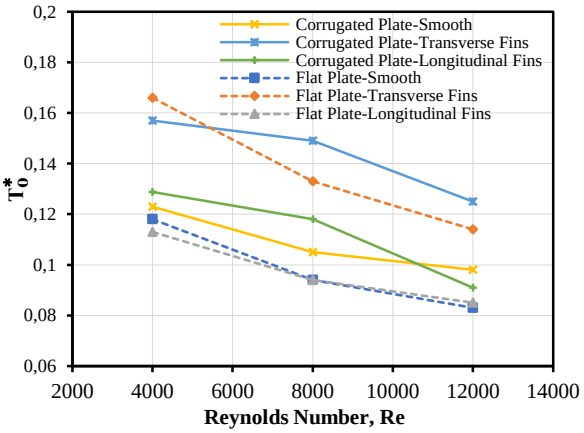

Figure 7. Non-dimensional outlet air temperature against Reynolds number

Nusselt Number

The average Nusselt number at different Reynolds numbers is presented in Figure 8 for different SAHs. It also presents Nusselt number results from the selected experimental studies for comparison. It is seen that the trends of Nusselt number obtained in the current numerical study is in good agreement with the experimental data. It should be noted that the experimental data are not meant for one to one comparison with the data obtained from the present study since the configuration used in the experimental studies are not identical to the configurations used in the current study. The graph shows that for all SAHs considered, increasing Reynolds number causes increase in Nusselt number due to the accompanied decrease in the thickness of the laminar sub-layer. For V-corrugated SAHs, the highest value of Nusselt number was obtained in transverse fins case which correspond to 45.8 at Re=12000. The transverse fins act as turbulators, they break the laminar sub-layer and generate secondary flow and reattachment region after the fin resulting in higher Nusselt numbers. In addition, the vortex flow generated by the fin contribute to the enhancement of local heat transfer by mixing and transporting the low temperature fluid in mid-duct to be in contact with the heated absorber plate. Figure 9 presents the velocity contour and reattachment region generated in the corrugated plate-transverse fins SAH. The lowest Nusselt number with value of 15.7 occurred in the longitudinal fins case at Re=4000.

It is important to note that the increase in Nusselt number alone is not the only factor to consider when evaluating the performance of a SAH. The overall thermal performance of the system, as well as the associated increase in friction factor, should also be taken into account. The results of this study suggest that the SAH with longitudinal fins was able to achieve a higher outlet temperature despite having lower Nusselt number values compared to the transverse fins SAH. This highlights the need for a balance between heat transfer enhancement and pressure drop in the design of SAHs. The next section of the paper provides further discussion on the friction factor.

For flat absorber SAHs, the highest Nusselt number was achieved in transverse fins case at Re=12000 with a value of 58.4. On the other hand, a Nusselt number of 19 corresponding to the minimum value was obtained in longitudinal fins case at Re=4000.

It is noted that for all Reynolds numbers considered the transverse fins case maintained the highest Nusselt numbers, while the longitudinal fins case produced the lowest values of Nusselt number. Therefore, it is apparent that the addition of roughness largely had the same effect on Nusselt number for both the flat and corrugated absorbers. Further investigation of the results suggests that the increase in Nusselt number that the transverse fins achieve over the smooth absorber SAH is higher in the case of flat absorber SAH than in the case of corrugated absorber SAH. This means that the difference in Nusselt number between the plate with transverse fins and smooth plate is considerably higher in the flat absorber plate SAH. Moreover, the decreases in average Nusselt number encountered by the addition of longitudinal fins was higher in the flat plate.

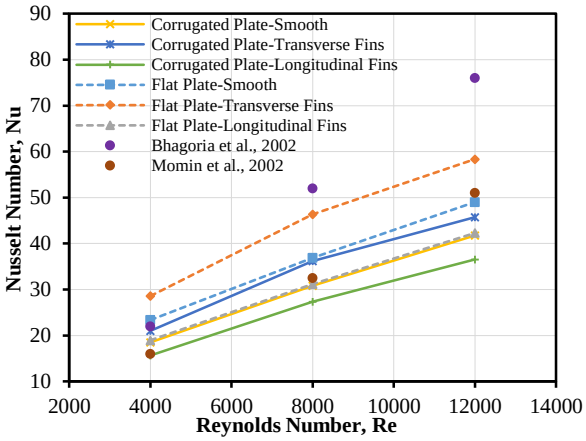

Figure 8. Nusselt number against Reynolds number for different SAHs

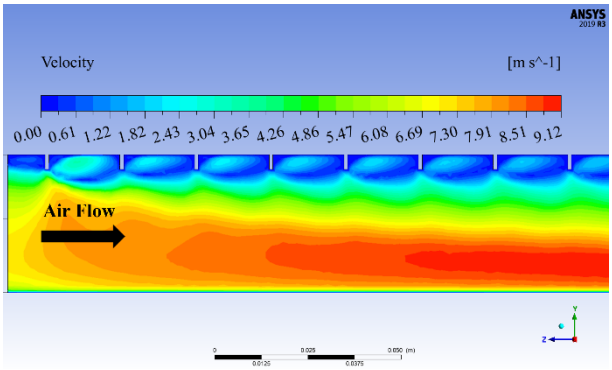

Figure 9. Contour of air velocity for corrugated plate-transverse fins SAH at Re=12000

Friction Characteristics

The average friction factor at different Reynolds numbers is plotted in Figure 10 for different SAHs. It can be observed that average friction factors are decreasing with increasing Reynolds number. It is thought that the

decrease in the friction factor is due to the termination of the laminar sub-layer encountered at rising Reynolds number.

For V-corrugated SAHs, the highest friction factor with value of 0.028 was achieved in transverse fins case as expected since the transverse fins have high flow resistance causing the pressure drop to increase. The smooth and longitudinal fins cases had close results for the average friction factor as seen in the graph. The minimum average friction factor occurred in the smooth case at Re=12000.

The friction factor represents a good reflection of the pumping power requirements of the SAHs since they share the same geometric characteristics; hydraulic diameter, length, etc. Generally, the addition of fins causes higher pressure-drop and hence higher pumping power. Therefore, the goal in SAH systems is to increase the outlet air temperature while keeping the pressure drop as low as possible. The addition of transverse fins on the corrugated plate resulted in an average friction factor of 0.0245 which is almost 2 folds that of the smooth case, while offering 1 degree increase in the outlet temperature compared to the smooth plate. On the other hand, the longitudinal fins generated an average friction factor of 0.0123 which is slightly higher than the that of the smooth case while offering up to 4 degrees increase in the outlet temperature as compared to the smooth plate. Therefore, the longitudinal fins represent a better alternative, since it resulted in higher outlet temperature with half of the pumping power requirement for the transverse fins.

For flat absorber SAHs, the maximum friction factor value occurred in transverse fins case at Re=4000, while the lowest value of the average friction factor occurred in the longitudinal fins case at Re=12000. The findings showed that for the average friction factor, the addition of fins had a similar effect in both flat absorber plate and corrugated absorber plate. Furthermore, a thorough investigation of the results suggests that the increase in the average friction factor caused by attaching transverse fins to a corrugated absorber is higher than the flat absorber case.

Figure 10 also presents the results of the friction factor from selected experimental studies for comparison. It can be observed that the trends of the friction factor obtained in the current numerical study match well with the experimental data.

In addition, Figure 10 shows a decrease in the friction factor by addition of longitudinal fins for the flat plate SAH, also the corrugated plate-smooth and corrugated plate-longitudinal fins achieved lower friction factor values than their flat plate counterparts. Although all SAHs were assigned with same uniform air velocity (hence the same Reynolds number) at the inlet section, the test sections' velocity distribution are different for different SAHs due to their geometrical differences (smooth, transverse fins, longitudinal fins) in the air channel. As illustrated in Figure 10, the friction factor is function of Reynolds number which is dependent on the velocity and higher Reynolds number (higher velocity) means lower friction factor. Addition of longitudinal fins to the flat plate SAH resulted higher velocities in the test section compared with the smooth one which is the reason for lower friction factor. This phenomenon can be observed in Figure 11. Similarly, corrugated plate smooth SAH experienced higher velocities than flat plate smooth SAH as shown in Figure 12 causing lower friction factor in corrugated plate smooth SAH. On the other hand, corrugated plate-longitudinal fins, and flat plate-longitudinal fins SAHs had similar velocity distribution in the test section as shown in Figure 13, which led to close friction factor values.

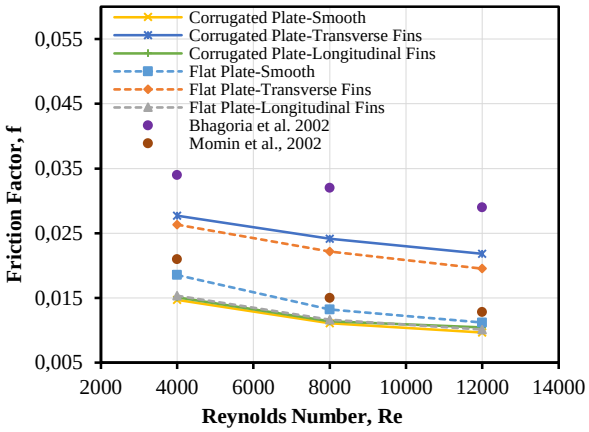

Figure 10. Friction factor against Reynolds number for different SAHs

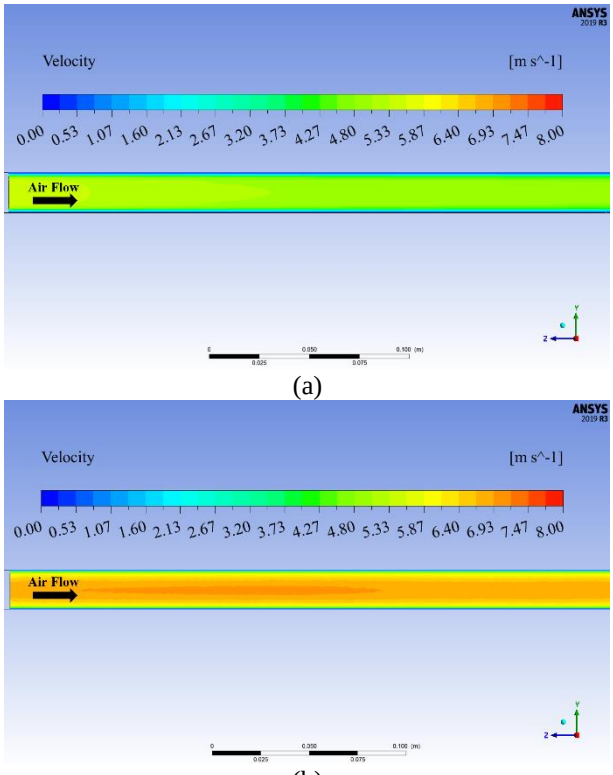

Figure 11. Velocity contour in the test section of (a) Flat plate-smooth (b) Flat plate-longitudinal fins SAHs

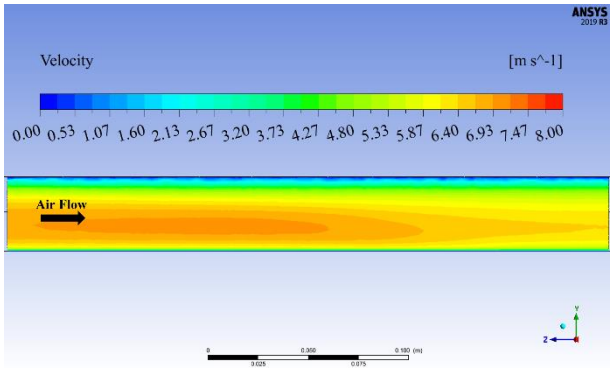

(a)

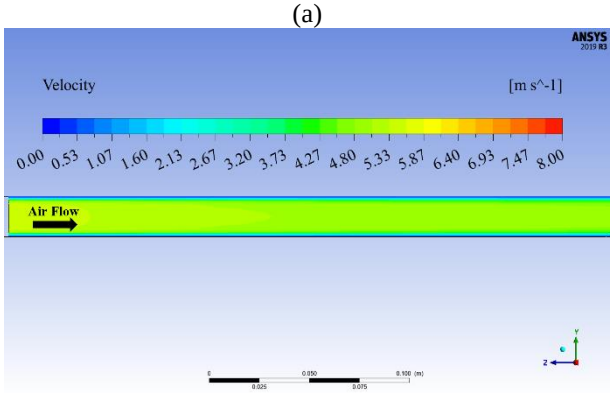

(b)

Figure 12. Velocity contour in the test section of (a) Corrugated plate-smooth (b) Flat plate-smooth SAHs

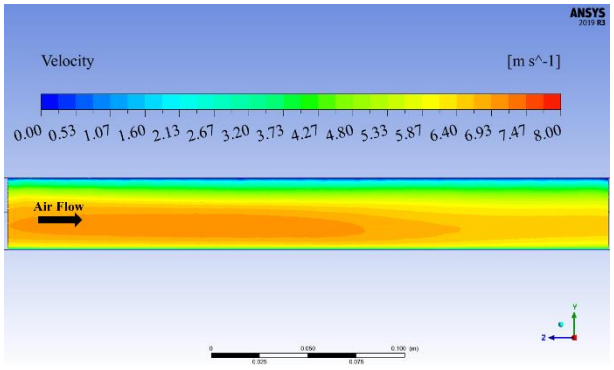

(a)

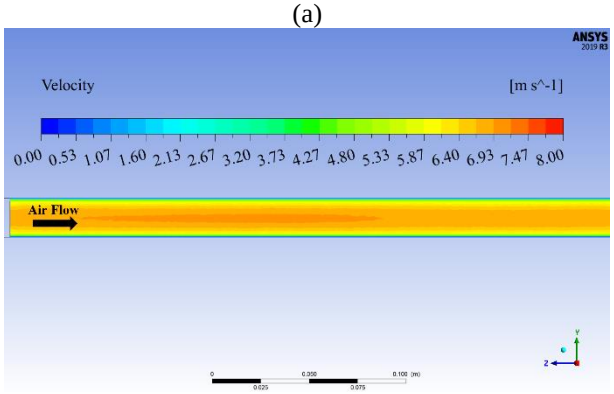

(b)

Figure 13. Velocity contour in the test section of (a) Corrugated plate-longitudinal fins (b) Flat plate-longitudinal fins SAHs

Figure 14 shows the pressure drop at different Reynolds numbers for the considered SAHs. It is seen from the figure that the pressure drop increases as Reynolds number increases. For different types of SAHs the pressure drop results follow similar fashion as the friction factor results, e.g. the maximum pressure drop and friction factor occurred in corrugated plate-transverse fins case, whereas minimum pressure drop and friction factor occurred in corrugated plate-smooth case. Simply it can be said that configuration with higher friction factor resulted in higher pressure drop.

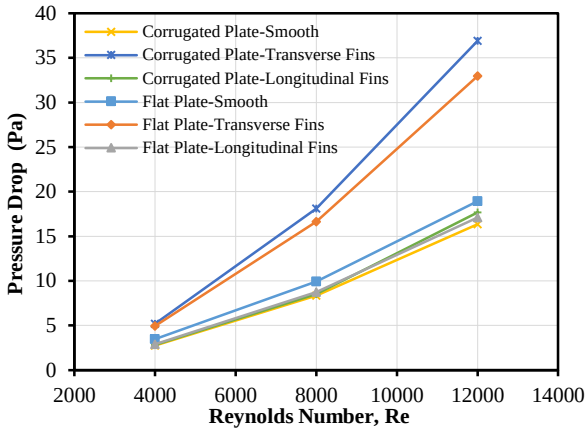

Figure 14. Pressure drop against Reynolds number for different SAHs.

CONCLUSION

The objective of this work is to numerically investigate the thermohydraulic performance of six SAHs; corrugated plate-smooth, corrugated plate-transverse fins, corrugated plate-longitudinal fins, flat plate-smooth, flat plate-transverse fins and flat plate-longitudinal fins, at different Reynolds numbers. Simplified three-dimensional model of each SAH was constructed by SolidWorks software, then the model was exported to ANSYS Fluent software to simulate and analyze the fluid flow inside the SAHs. The required setting and methods for solving the governing equations and to model turbulence were set. An appropriate mesh was generated for each SAH and required boundary conditions were assigned to the different surfaces in the computational domain.

The results showed that the maximum outlet air temperature was 315.32 K in the corrugated plate-longitudinal fins SAH at Re=4000, while the minimum outlet air temperature was 302.27 K in the flat plate-smooth SAH at Re=12000. In addition, the findings showed a considerable improvement in the average Nusselt number by attaching transverse fins to the absorber plate. The highest obtained average Nusselt number was 58.37 in the flat plate-transverse fins SAH at Re=12000, while the minimum average Nusselt number occurred in the corrugated plate-longitudinal fins SAH with a value of 15.67 at Re=4000. Similarly, a noticeable friction factor increase was found in SAHs with transverse fins. The maximum average friction factor was 0.0277 in the corrugated plate-transverse fins SAH at Re=4000. On the other hand, the minimum average

friction factor was obtained in the smooth corrugated plate SAH at Re=12000 and with a value of 0.0097.
The corrugated plate-longitudinal fins SAH was found to be the most effective configuration. It was able to achieve the highest outlet temperature with lower friction factor values. Moreover, the addition of each roughness elements; transverse fins and longitudinal fins is observed to have generally a similar effect on the thermohydraulic performance of the two SAHs types considered. The results show that the enhancement in Nusselt number that the transverse fins provide compared to the smooth absorber SAH is greater in the case of the flat absorber SAH than in the case of the corrugated absorber SAH. In addition, the results suggest that the average friction factor is increased more by attaching transverse fins to a corrugated absorber than to a flat absorber.

The manufacturing aspect of the proposed SAHs with roughness elements is important to consider as it could result in added cost which may not be justified by the improvement in performance. Therefore, further investigation is needed to fully understand the feasibility of implementing the proposed SAH configurations in practical systems, which is out of the scope of the current study. However, the authors suggest the use of thermally conductive adhesives as a potential practical solution for attaching roughness elements to a corrugated absorber. This could be investigated in future work.

REFERENCES

ANSYS, 2013, *Ansys Fluent Theory Guide 15.0*, ANSYS Inc., Canonsburg.

Arunkumar, H. S., Vasudeva Karanth, K., and Kumar, S., 2020, Review on the design modifications of a solar air heater for improvement in the thermal performance, *Sustainable Energy Technologies and Assessments*, *39*, 100685.

Bhagoria, J. L., Saini, J. S., and Solanki, S. C., 2002, Heat transfer coefficient and friction factor correlations for rectangular solar air heater duct having transverse wedge shaped rib roughness on the absorber plate, *Renewable Energy*, *25*(3), 341–369.

Farhan, A. A., Issam M.Ali, A., and Ahmed, H. E., 2021, Energetic and exergetic efficiency analysis of a v-corrugated solar air heater integrated with twisted tape inserts, *Renewable Energy*, *169*, 1373–1385.

Gawande, V. B., Dhoble, A. S., Zodpe, D. B., and Chamoli, S., 2016, Experimental and CFD-based thermal performance prediction of solar air heater provided with chamfered square rib as artificial roughness, *Journal of the Brazilian Society of Mechanical Sciences and Engineering*, *38*(2), 643–663.

Ghritlahre, H. K., Chandrakar, P., and Ahmad, A., 2019, A Comprehensive Review on Performance Prediction of Solar Air Heaters Using Artificial Neural Network. In *Annals of Data Science* , 8, 405-449.

Handoyo, E. A., Ichsani, D., Prabowo, and Sutardi., 2016, Numerical studies on the effect of delta-shaped obstacles' spacing on the heat transfer and pressure drop in v-corrugated channel of solar air heater, *Solar Energy*, *131*, 47–60.

Incropera, F. P., and DeWitt, D. P., 2007, *Fundamentals of Heat and Mass Transfer* (Sixth Edition), Wiley, New York.

Jiji, L. M., 2009, *Heat convection* (Second Edition), Springer, New York.

Jin, D., Zhang, M., Wang, P., and Xu, S., 2015, Numerical investigation of heat transfer and fluid flow in a solar air heater duct with multi V-shaped ribs on the absorber plate, *Energy*, *89*, 178–190.

Kumar, Amit, and Layek, A., 2021, Energetic and exergetic based performance evaluation of solar air heater having winglet type roughness on absorber surface, *Solar Energy Materials and Solar Cells*, *230*, 111147.

Kumar, Anil, and Kim, M. H., 2015, Effect of roughness width ratios in discrete multi V-rib with staggered rib roughness on overall thermal performance of solar air channel, *Solar Energy*, *119*, 399–414.

Kumar, M., and Mr, V., 2014, A Computational Fluid Dynamics Investigation of Solar Air Heater Duct Provided with Inclined Circular Ribs as Artificial Roughness, *Bonfring International Journal of Industrial Engineering and Management Science*, *4*, 115–120.

Momin, A.-M. E., Saini, J., and Solanki., S., 2002, Heat transfer and friction in solar air heater duct with V-shaped rib roughness on absorber plate. *International Journal of Heat and Mass Transfer*, *45*(16), 3383–3396.

Parsa, H., Saffar-Avval, M., and Hajmohammadi, M. R., 2021, 3D simulation and parametric optimization of a solar air heater with a novel staggered cuboid baffles, *International Journal of Mechanical Sciences*, *205*, 106607.

Poongavanam, G. K., Panchabikesan, K., Leo, A. J. D., and Ramalingam, V., 2018, Experimental investigation on heat transfer augmentation of solar air heater using shot blasted V-corrugated absorber plate, *Renewable Energy*, *127*, 213–229.

Prasad, B. N., and Saini, J. S., 1988, *Effect of artificial roughness on heat transfer and friction factor in a solar air heater*. *41*(6), 555–560.

Saini, R. P., and Saini, J. S., 1997, Heat transfer and friction factor correlations for artificially roughened

ducts with expanded metal mesh as roughness element, *International Journal of Heat and Mass Transfer*, *40*(4), 973–986.

Saini, R. P., and Verma, J., 2008, Heat transfer and friction factor correlations for a duct having dimple-shape artificial roughness for solar air heaters, *Energy*, *33*(8), 1277–1287.

Saxena, A., Varun, and El-Sebaii, A. A., 2015, A thermodynamic review of solar air heaters, *Renewable and Sustainable Energy Reviews*, *43*, 863–890.

Singh Bisht, V., Kumar Patil, A., and Gupta, A., 2018, Review and performance evaluation of roughened solar air heaters, *Renewable and Sustainable Energy Reviews*, *81*, 954–977.

ASHRAE, 2003, *Methods of testing to determine the thermal performance of solar collectors*, American Society of Heating, Refrigerating, and Air-Conditioning Engineers, Atlanta.

Sureandhar, G., Srinivasan, G., Muthukumar, P., and Senthilmurugan, S., 2021, Performance analysis of arc rib fin embedded in a solar air heater, *Thermal Science and Engineering Progress*, *23*, *100891*.

Tyagi, V. V., Panwar, N. L., Rahim, N. A., and Kothari, R., 2012, Review on solar air heating system with and without thermal energy storage system, *Renewable and Sustainable Energy Reviews*, *16*(4), 2289–2303.

Yadav, A. S., and Bhagoria, J. L., 2014a, A CFD based thermo-hydraulic performance analysis of an artificially roughened solar air heater having equilateral triangular sectioned rib roughness on the absorber plate, *International Journal of Heat and Mass Transfer*, *70*, 1016–1039.

Yadav, A. S., and Bhagoria, J. L., 2014b, A numerical investigation of square sectioned transverse rib roughened solar air heater. *International Journal of Thermal Sciences*, *79*, 111–131.

Yakhot, V., and Smith, L. M., 1992, The renormalization group, the ε-expansion and derivation of turbulence models, *Journal of Scientific Computing*, *7*(1), 35–61.